Journal of Nuclear Materials 394 (2009) 166–173

Contents lists available at ScienceDirect

Journal of Nuclear Materials

journal homepage: www.elsevier.com/locate/jnucmat

Thermal reactions of uranium metal, UO_2, U_3O_8, UF_4, and UO_2F_2 with NF_3 to produce UF_6

Bruce McNamara *, Randall Scheele, Anne Kozelisky, Matthew Edwards

Pacific Northwest National Laboratory, Richland, WA 99352, USA

ARTICLE INFO

Article history:
Received 4 September 2008
Accepted 12 September 2009

ABSTRACT

This paper demonstrates that NF_3 fluorinates uranium metal, UO_2, UF_4, UO_3, U_3O_8, and $UO_2F_2{\cdot}2H_2O$ to produce the volatile UF_6 at temperatures between 100 and 550 °C. Thermogravimetric and differential thermal analysis reaction profiles are described that reflect changes in the uranium fluorination/oxidation state, physiochemical effects, and instances of discrete chemical speciation. Large differences in the onset temperatures for each system investigated implicate changes in mode of the NF_3 gas–solid surface interaction. These studies also demonstrate that NF_3 is a potential replacement fluorinating agent in the existing nuclear fuel cycle and in actinide volatility reprocessing.

1. Introduction

This paper provides the results of thermoanalytical investigations and thermodynamic considerations of nitrogen trifluoride (NF_3) as a fluorinating agent for uranium compounds. Fluorination technologies have been used historically to enrich ^{235}U from various uranium feedstocks by gaseous diffusion [1–3] and have been discussed for nuclear fuels recycle [4–6], nuclear materials separations [7], purification [1,8], and US Department of Energy (DOE) site decontamination [9,10]. With respect to nuclear materials separations, the hexafluorides of U, Pu, and Np can be separated from complex matrices and each other by their volatility and the physical properties (boiling point, sublimation point) of the gaseous products. Large-scale fluorination processes typically have depended on using potent fluorination reagents that are hazardous to human health, environmentally intrusive, and expensive to produce, transport, and store. The reaction kinetics of several of these F_2 [11–16], ClF_3 [15], $BrCl_3$ [16], O_2F_2 [17–20], KrF_2 [20,21] have been investigated with regard to their utility as uranium and actinide fluorinating reagents.

An alternative fluorinating reagent, NF_3, is currently used to etch and clean microelectronic devices [22–25]. The reagent is not corrosive and does not react with moisture, acids, or bases at room temperature. NF_3 is thermally stable to relatively high temperatures and is also insensitive to shock to pressures above 1,00,000 psi [26] so that reduced economics associated with transportation, storage, and everyday laboratory or large-scale processes are realized.

Successful etching of UO_2 in NF_3 glow discharge experiments has been discussed [27,28]. The utility of this process may be limited for large-scale process work because of the small footprint of the radiofrequency (RF) apparatus and the need to operate under a significant vacuum, but it is clear that removing uranium and other transuranics can be made quite effective.

Uranium hexafluoride (UF_6) is a white volatile solid that sublimes at 57 °C. At room temperature, the vapor pressure of UF_6 is about 0.14 atm, and this increases to about 13.6 atm near 150 °C. The high vapor pressure of UF_6 and the fact that it is the only appreciably volatile product derived from the fluorination of uranium materials below 700 °C [29] are properties historically advantageous to the study of fluorination of uranium using thermal gravimetric methods.

Signatures generated from differential thermal analysis and thermogravimetric experiments are inadequate for probing detailed mechanistic issues in reactive chemical systems other than supporting or disproving hypothesized reactions, but can be used to observe chemical or physiochemical transformations that occur with heating of a sample. Characteristic of these are, endothermic and exothermic heat exchange, primary and secondary changes in crystallinity and phase, evolution or adsorption of gas to produce mass change, formation of product barriers and discrete chemical intermediates formation. While the temperature onset and regions of stability for intermediate products might be established using TGA, the goal of their isolation and identification can met by application of other techniques more suited to that purpose. Because the reactivities of NF_3 and fluorine gas with uranium materials are in several ways similar, the extensive literature concerning uranium fluorination was considered to help identify more obvious chemical intermediates involved in the various fluorination sequences.

* Corresponding author. Tel.: +1 509 376 7015; fax: +1 509 373 9675.
E-mail address: bruce.mcnamara@pnl.gov (B. McNamara).

0022-3115/$ - see front matter © 2009 Elsevier B.V. All rights reserved.
doi:10.1016/j.jnucmat.2009.09.004

For the experiments discussed here, variation of the sample heating rate is broadly used to map out thermal behaviors in the reactions of NF_3 with several uranium compounds. The selection of the heating rate generally determines the onset temperature for a given event and can often be chosen to resolve events that might overlap on the temperature axis. The chosen scan rates displayed throughout the text are based on several tens of trials for each system, from which we have selected the most resolved data to illustrate the sequential reactions that eventually produce UF_6. With this data set, we describe several evidences of deviation from the reported reactivity for F_2 gas with in particular UO_2, U_3O_8 and UF_4. It is not yet known if such differences are a function of the NF_3 reactivity or perhaps reflect a difference in experimental approach and reporting. Regardless, we observe complex behavior that is challenging to readily understand from the perspective of the known speciation involved in UF_6 production from these materials. Thermodynamic data are provided to emphasize the favorability of the conversion of a uranium compound by NF_3 to UF_6 or departures from expected behaviors. A goal of this report is to display such behavior with the intent of beginning a dialogue concerning the fundamental reactivity and applicability of NF_3.

2. Experimental methods

Uranium metal—UO_2, $UF_4{\cdot}2H_2O$, $UO_2F_2{\cdot}2H_2O$, UO_3, and α-U_3O_8—from house stocks at Pacific Northwest National Laboratory were characterized before their use by X-ray diffraction (XRD) on a Scintag (PAD III) diffractometer and by scanning electron microscopy (SEM) on a JOEL JEM 840S, with Oxford Instruments energy-dispersive spectroscopy (EDS). XRD spectra were obtained over a range from 5° to 65° 2θ with 0.02-degree-step sizes and a dwell time of 8 s/step. XRD powder patterns of $UF_4{\cdot}2H_2O$, UO_3, and U_3O_8, and $UO_2F_2{\cdot}2H_2O$ were acquired and were consistent with those in the International Centre for Diffraction Data (ICDD) database [30].

The XRD powder pattern of the stock UO_2 indicated the presence of a primary corrosion phase, metaschoepite $[(UO_2)_4O(OH)_6](H_2O)_5$ on/in the surface of the UO_2 particles. Thermogravimetric analysis (TGA) of the UO_2 confirmed the presence of less than 2 wt% of the hydrate.

SEM micrographs of NIST traceable α-U_3O_8 showed it to be 1 or 2 μm-sized nodular looking particles or aggregates of these that on closer examination had hexagonal appearance. β-U_3O_8 was prepared by heating the α-U_3O_8 powder to 1350 °C for 24 h [31] and slowly quenching the heat at a rate of 100 °C/day. The material was brittle and had a highly reflective appearance. The XRD of the material was consistent with the presence of some residual α-U_3O_8 mixed with the β-U_3O_8. SEM micrographs of the β-U_3O_8 indicated that the distinct particles were elongated relative those in the parent α-U_3O_8. The particle size increased considerably relative to the parent and ranged from 1 or 2 μm-sized particles to 200 μm pieces.

Uranium metal in the form of spheres approximately 1 mm in diameter had a geometric surface area of 0.0236 cm^2/g. An SEM micrograph indicated that the uranium metal surface had a very slight oxide layer on it. The metal was treated with three hydride/dehydride cycles in 4% H_2/Ar gas to 99.9% yield UH_3 by TGA indicating a similar purity of metal. An SEM micrograph indicated that the stock UO_2 particles were discrete with a particle size ranging from 10 to 75 μm.

The $UF_4{\cdot}2H_2O$ stock solids had been recrystallized from solution and the UO_3 stock had been prepared from thermal decomposition of uranyl peroxide and was actually a mixture of UO_3 and hydrated forms of UO_3. SEM micrographs of $UF_4{\cdot}2H_2O$ and the UO_3 samples showed that particles appeared as approximately 20-μm aggregates comprised of submicron particles.

Details of the method of preparation of $UO_2F_2{\cdot}2H_2O$ and characterizations of the product have been previously described [10]. SEM micrographs of the material indicated well-defined platy particles with a size distribution from 10 to 40 μm.

2.1. Thermogravimetric/differential thermal analysis

A combination thermogravimetric (TG) and differential thermal analysis (DTA) unit (Seiko model 350) was modified to accommodate NF_3 to temperatures in excess of 1000 °C. For this purpose, the normal path for passage of purge gases was modified with a $^1/_{16}$-in. (OD) nickel tube that was inserted to within 1 in. of the centre of the sample. The tube was used to both pre-heat the NF_3 gas and deliver it directly to the sample. A back pressure of argon gas was maintained to dilute the NF_3 concentration during sample exposure and also to avoid NF_3 backflow to electronic components residing inside the analytical balance area of the TG/DTA unit. Calibrated flow controllers were used to adjust the NF_3 and argon concentrations.

Samples were run in (99.999% Al) aluminum or gold pans purchased from Thermo Scientific (Waltham, MA). The sample and reference pans were pretreated for 1 h with NF_3 at 500 °C to passivate their surfaces and prevent small mass changes caused by their fluoridation during TG/DTA analyses. Samples were run in isothermal mode between 100 and 500 °C and under heat-ramp conditions at 1, 2, 5, 10, and 20 °C min^{-1}. Mass (TG) and heat flow (DTA) baselines were run under the same conditions as the samples to establish the instrument response over the time and temperature range of the thermal experiments. Mass changes to ± 5 μg were considered acceptable in the mass baseline. Fluctuations below ± 20 microvolts were considered acceptable in the DTA baseline.

For the reaction of NF_3 and $UO_2F_2{\cdot}2H_2O$ only a Nicolet 750 infrared (IR) spectrometer was used to qualitatively identify IR-active evolved gases from these TG/DTA experiments.

The enthalpies and free energies of formation of UF_6 from the reaction between NF_3 and several uranium compounds were calculated using a chemical reaction and equilibrium software package; HSC Chemistry® [32]. Thermodynamic data are reported in Table 1 at a median temperature of 300 °C as the calculated values did not change more than 10% between 200 and 500 °C. The thermodynamic calculations provide a measure of whether a reaction is favorable or not.

3. Results and discussion

The reactions of NF_3 with uranium metal, its oxides, and fluorides to produce volatile UF_6 are predicted to be exothermic and in general are observed to be exothermic. The use of a purge gas in the TG/DTA experiments complicates the measurement of exothermic reaction heats through removal of the chemically heated gas from the system and the effective removal of UF_6 gas as it is formed. Some of the latent heat of UF_6 formation is concomitantly removed from the instrument's thermal detection systems to the extent that the experimental enthalpies of exothermic reactions can not be measured with certainty. The same holds true for the exothermic formation of UF_4 from uranium metal, UO_2F_2 from

Table 1
Enthalpies and free energies per mol uranium for reaction of NF_3 for the overall reactions of selected uranium oxides, UF_4 and UO_2F_2 to produce UF_6.

Eq.	Overall reaction to UF_6	ΔH (kJ/mol U)	ΔG (kJ/mol U)
1	$UO_2 + 2NF_{3(g)} = UF_{6(g)} + N_{2(g)} + O_{2(g)}$	−799.9	−901.1
2	$UO_2F_2 + NF_{3(g)} = UF_{6(g)} + N_{2(g)} + O_{2(g)}$	−321.2	−448.8
3	$UO_3 + 2NF_{3(g)} = UF_{6(g)} + N_{2(g)} + O_{2(g)}$	−661.9	−809.8
4	$U_3O_8 + 6NF_{3(g)} = 3UF_{6(g)} + 3N_{2(g)}+$	−695.2	−823.2
5	$UF_4 + NF_{3(g)} = UF_{6(g)} + N_{2(g)}$	−144.1	−204.9
6	$U + 2NF_{3(g)} = UF_{6(g)} + N_{2(g)}$	−1881.9	−1884.8

UO_2, etc. The effect can reduce the recorded heats to zero intensity and might for instance occur if the purge rate exceeded the rate of heat production of the reactive system.

Coupled to complexity of the NF_3/uranium interaction such empirical deception can conspire to make interpretation of the thermal data presented herein challenging. Some guidance can be provided by thermodynamic modeling of the chemical systems involved. The enthalpies and free energies of formation of UF_6 from the reaction between NF_3 and several uranium compounds were calculated and are reported in Table 1. For these calculations, the stoichiometric lowest energy product distributions were postulated for metrical purposes. It should not be construed that these are actual product distributions, however, UF_6, N_2 and O_2 are the products in fact observed using RF field excitation of NF_3 for UF_6 production from UO_2 [27]. The thermodynamic calculations predict overall exothermic conversion of uranium compounds to UF_6 and do so even using various product distributions that would result in stoichiometric NO_x production. Accordingly, the exothermic behavior so accounted for should be an observable in the thermoanalytical results.

Based on the thermodynamic data for U metal, UO_2, U_3O_8, UO_3, UO_2F_2, and UF_4 in Table 1, one would conclude that there is a correlation of the uranium oxidation state with the heats of reaction produced during the fluorination process. The overall trend is compiled in Table 2 and this trend should also be an observable in the experimental data. While seemingly obvious, as for instance it is somewhat analogous to the more well-studied oxidation reactions of these uranium compounds, the trend is in fact experimentally defied by two cases in particular; those of U_3O_8 and UF_4. Each display endothermic mass loss (as UF_6) especially at low sample heating rate. While our understanding of this behavior is presently limited, the thermodynamic calculations at least point us away from an explanation that is based on a change in the (known) intermediates of fluorination, and towards one involving a decomposition, or other event(s) that is endothermic in nature and apparently emphasized by the choice of sample heating rate.

With respect to the issue of product distribution, the decomposition of NF_3 gas or its thermal reaction with uranium oxides for instance could lead to nitrogenous primary or side products. Experiments evaluating NF_3 plasma as an etchant for SiO_2 [22–25] and uranium materials [27,28] have been carried out in apparatus designed to scrupulously avoid air and moisture and production of side products, e.g. HF, and nitrogen oxides are not reported. While the thermogravimetric experiments reported here were purged in argon, it is clear that the reactivity of thermally activated NF_3 above 350 °C is such that simple purging is not adequate to completely reduce emission of such products from our experiments. In several experiments, the presence of small amounts of HF and NO_2 were detected by IR. Because these product concentrations did not dominate the infrared spectra, it was surmised that such products were formed through adventitious hydrolysis of reaction products (UF_6) or of thermally activated NF_3 with opportunistic air (O_2) on surfaces inside and exiting the furnace of the TG apparatus as opposed to being primary reaction products.

3.1. NF_3 fluorination of UO_2

The overall reaction to produce UF_6 from reaction of F_2 with UO_2 is considered in the literature to be a two step process [33]. The reaction with NF_3 is listed in Table 1: Eqs. (1) and (2). The general observation is that UO_2F_2 is formed preferentially to UF_6 unless the sample heating rate or reaction heat forces a rapid increase in temperature that drives production of UF_6. This is true to the extent that the entire UO_2 sample can be isothermally converted to UO_2F_2 near 400 °C. The result allows a purely thermal synthesis of UO_2F_2 (anhydrous) from UO_2.

Fig. 1(a) and (b) show the TG/DTA scans of samples of UO_2 powder exposed to a flow of 5% NF_3 in argon gas at two different sample heating rates. The selection of the heating rate was used to resolve thermal signatures of chemical speciation or of physiochemical changes in the reacting system. The sample heating rate used in Fig. 1a was 5 °C min^{-1}. The reaction profile shown in Fig. 1b resulted from a heating rate of 20 °C min^{-1}. The DTA scan in Fig. 1a shows three discrete exothermic events (marked 1, 2, and 3) as $U^{(IV)}O_2$ was converted to UF_6. In Fig. 1a slight mass gain began near 200 °C and continued to about 457 °C. The total mass increase was consistent with complete conversion of the UO_2 sample to $UO_2F_{2(anhydrous)}$ to within 0.02 wt%.

The reaction was quenched by cooling the sample near 440 °C to room temperature under the NF_3/argon purge. An XRD powder pattern acquired from the sample confirmed the presence of UO_2F_2 as the only air-stable product. This quenching experiment may be confounded by the instability of higher uranium fluorides when exposed to air and moisture and potential conversion to UO_2F_2 as the sample is recovered and mounted for XRD analysis, e.g., UF_6 reacts with water to form UO_2F_2. The mass change and XRD analysis support that the first sharp exotherm in Fig. 1a was caused by the fluorination of UO_2 to UO_2F_2.

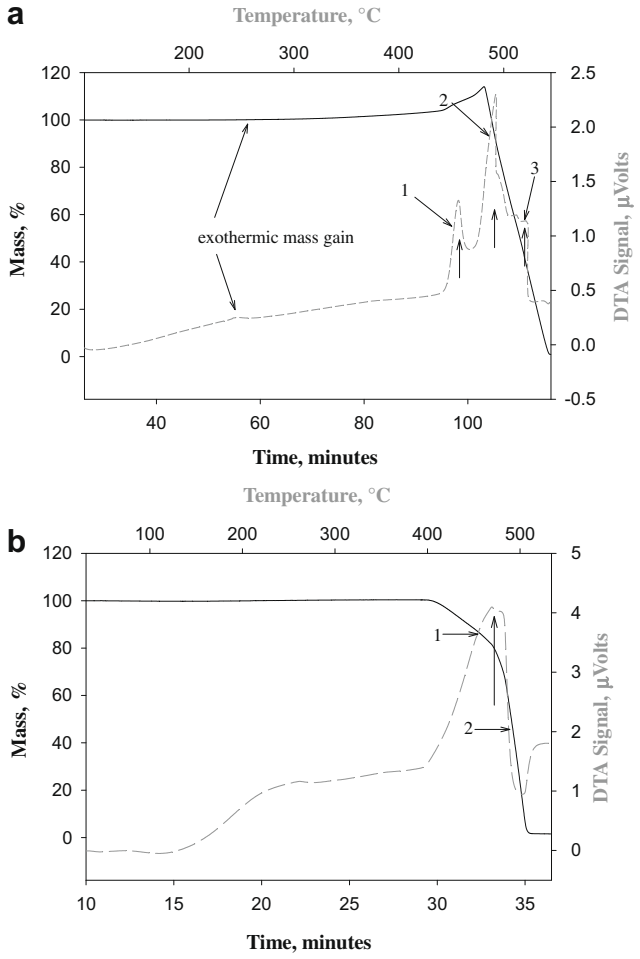

Fig. 1. (a) Thermal profile for the reaction of UO_2 powder and NF_3 as measured by TG/DTA at a heating rate of 5 °C min^{-1}. At this sample heating rate, three thermal events (marked) were observed. (b) The thermal profile for the reaction of UO_2 powder and NF_3 as measured by TG/DTA at a heating rate of 20 °C min^{-1}. The increased heating rate resolved two discrete decomposition rates. The mass (TG) curves are plotted as the solid lines, and the DTA curves are the dashed lines. Exothermic reactions exhibit an increase in the heat flow and are indicated by the up arrow.

The mass increase was followed by rapid, exothermic mass loss, indicating release of UF_6 near 492 °C, until 100% of the sample was volatilized. On the high-temperature side of the DTA curve, a feature (marked 3) indicates that at least one other chemical species or other thermal event was involved in the release of UF_6. The presence of a third exothermic event has not been cited for fluorination of UO_2 with use of other fluorinating reagents (33).

The higher heating rate 20 °C/min, displayed in the TGA scan in Fig. 1b, does not show the mass buildup of UO_2F_2 because the increased sample heat rate accelerated heat and mass transport throughout the sample. In the mass-loss portion of the TG curve, two distinct rate contributions marked (1) and (2) in Fig. 1b comprise the release of UF_6. The higher heating rate allows observation of a rate-limited region (1), suggestive of formation of a product or product barrier, and a region (2) of more facile UF_6 production. These data are aptly described by gas–solid models developed recently for fluorination UO_2 (33) by F_2.

It is not yet understood if the third exotherm as shown in Fig. 1a was a chemically distinct product or was rather due to physical changes in the evolving sample. Intermediate products of uranium oxide fluorination that have been identified in the literature include UOF_4 [34–38], $U_2O_3F_6$ [39], and $U_3O_5F_8$ [40]. The distinctive orange coloration of UOF_4 and $U_3O_5F_8$ [34,40] has not been observed in our (quenched) experiments. The rate limiting aspect of the data in Fig. 1b could be explained by the presence of a quickly formed rind(s) of UO_2F_2 or other fluorinated product barrier, brought on by the fast ramp rate and whose fluorination to UF_6 would be also exothermic but might slow the rate of NF_3 penetration or UF_6 release.

3.2. NF_3 fluorination of UO_2F_2

The thermal reaction of UO_2 and NF_3 was confirmed above to produce $UO_2F_{2(anhydrous)}$. SEM micrographs of the fully converted samples showed that the particles of UO_2F_2 were pulverized to about 100 nm with respect to the UO_2 particles. Fig. 2 shows the thermal reactivity of a synthetic crystalline $UO_2F_2{\cdot}2H_2O$ powder exposed to a flow of 5% NF_3 in argon. The thermal scan is consistent with those discussed in available literature concerning the fluorination of UO_2F_2. The initial mass loss in Fig. 2 is caused by thermal loss of waters of hydration. This event was complete near 300 °C where the NF_3 was turned on. Sample heat rates set at 2 °C min^{-1} allowed mass losses near 300 °C that corresponded to the formation of UF_6 to be observed. The rate of release of UF_6 increased to

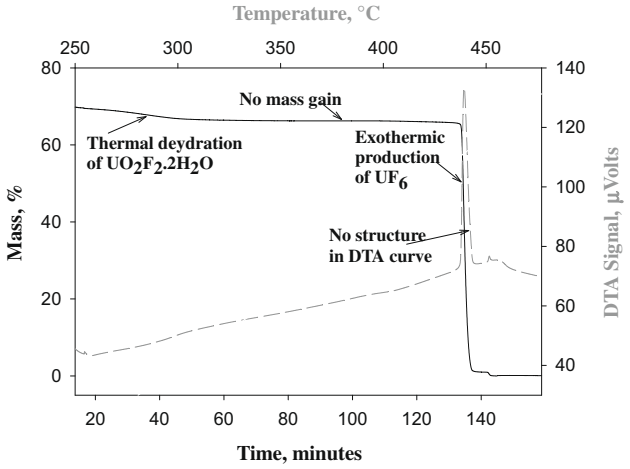

Fig. 2. The TG/DTA-measured thermal profile of UO_2F_2 with NF_3 at a heating rate of 2 °C min^{-1}. The experimental TG curves are plotted as solid lines, and the DTA curves are dashed lines. Exothermic reactions exhibit an increase in the heat flow.

near 470 °C and was accompanied by rapid self-heating of the sample to 550 °C. These observations are generally consistent with those described in Fig. 1a and b for intermediate formation of $UO_2F_{2(anhydrous)}$ in the reaction of NF_3 with UO_2.

There were some differences between the overall fluorination of UO_2 and the synthetic $UO_2F_2{\cdot}2H_2O$. For all sample heating rates used for the fluorination of $UO_2F_2{\cdot}2H_2O$, only the single exothermic feature (see Fig. 1a) was apparent in the DTA scan in the region of UF_6 formation. Mass gains observed for UO_2 (see Fig. 1a and b), that would indicate the transient formation of uranium fluorides to intermediates such as UOF_4 [34–38], $U_2O_3F_6$ [39], and $U_3O_5F_8$ [40], were not observed for the synthetic $UO_2F_2{\cdot}2H_2O$ at any sample heat rate, or for a large set of isothermal scans between 300 to 450 °C. The third exotherm seen in Fig. 1a was also not observed at any heating rate. These differences point to a structural or other difference between our two sources of UO_2F_2; one as thermally prepared from reaction of NF_3 and UO_2 and the other crystallized from solution as $UO_2F_2{\cdot}2H_2O$.

Direct sublimation of UO_2F_2 is a potential mechanism for its mass loss and this would appear as a change in the mass loss rate. The vapor pressure of UO_2F_2 at 1030 K is 1.2×10^{-5} atm [35].

$$UO_2F_{2(s)} = UO_2F_{2(g)} \quad (1)$$

so that the vapor pressure between 300 and 470 °C would be too low to contribute to any observable mass loss in our experiments. Decomposition reactions such as (2) that would form U_3O_8 were initially dismissed as contributing to mass loss on the basis that U_3O_8 is stable and

$$3UO_2F_{2(s)} = UF_{6(g)} + 1/3O_{2(g)} + 2/3U_3O_{8(s)} \quad (2)$$

quenched isothermal experiments, run from 300 to 470 °C, did not exhibit by XRD any evidence of U_3O_8 formation. From Table 2 it can be seen that the free energy of fluorination of U_3O_8 is more favorable than that of UO_2F_2 so that such reactions may not be excluded without consideration of further evidences.

Two plausible explanations of the difference in reactivity of what appears to be the same compound is that during the fluorination of UO_2 to UO_2F_2, (1) some oxidizing of the UO_2 to $UO_{(2+x)}$ could lead to different uranium fluoride speciation and (2) the UO_2 particle features (i.e., crystallinity, porosity) annihilated by fluorination could lead to higher fluoriding per mass of sample than can occur on well formed particles of the chemically prepared UO_2F_2. SEM micrographs of the thermally produced material indeed showed that the UO_2 (10–75 μm) had been pulverized by the treatment with NF_3, with the final UO_2F_2 product having 100 nm-sized (but still crystalline) particles, compared to the chemically prepared, crystalline particles of $UO_2F_2{\cdot}2H_2O$ (40 μm).

A final note concerning conversion of hexavalent UO_2F_2 to UF_6 was that the exothermicity predicted in Table 1 was easily observable at all sample heating rates, even though the calculated enthalpy was lower than UO_3 and U_3O_8.

Table 2
Correlation of uranium oxidation state with enthalpies and free energies per mol uranium. The free energy of formation for the staring uranium compounds are listed in the 2nd column.

U phase	ΔG_{form} (kJ/mol U)	ΔH_{Rxn} (kJ/mol U)	ΔG_{Rxn} (kJ/mol U)
U^0	0	−1881.9	−1884.8
UO_2	−983	−799	−901
U_3O_8	−1061	−695	−823
UO_3	−1075	−662	−809
UO_2F_2	−1470	−320	−446
UF_4	−1748	−144	−205

3.3. NF_3 fluorination of UO_3

Reactions of NF_3 with UO_3 exhibited reactivity at a lower temperature than either UO_2 or UO_2F_2. The overall reaction stoichiometry as postulated in Table 1, Eq. (3) suggests a lower enthalpy for formation of UF_6 relative to UO_2. Fig. 3 shows the TG/DTA-measured thermal reactivity of a sample of $U^{(VI)}O_3$ powder exposed to a flow of 5% NF_3 in argon. At a sample heating rate of 2 °C min^{-1}, both the DTA and the TG curves indicated the presence of two discrete UF_6-producing regimes, which are marked (1) and (2) in Fig. 3. UF_6 production is the only possibility for mass loss and this occurred as low as 275 °C at an appreciable rate. At higher ramp rate, the two events coalesced into one UF_6 release event.

With respect to F_2 fluorination of UO_3 [12], UO_2F_2 has been suggested to be one of the intermediates in the fluorination of UO_3. By comparison, it is reasonable to suspect the same occurs for the NF_3 reaction with UO_3. This leaves open the question as to the nature of the other thermal signature for which there is no reported instance of in the fluorination literature. Consequently, it is not know if the first signature is particular to NF_3 versus F_2 gas reactivity or if a difference in experimental approach is the origin of the result. Because the formation of UO_2F_2 from UO_2 is thermodynamically favored relative to its formation from UO_3, it would seem the lower temperature exotherm (275 °C) should be due to formation of some other intermediate than the production of UF_6 from UO_2F_2 (300 °C), such as $U_2O_3F_6$ [39] or $U_3O_5F_8$ [40]. The higher fluoride content in these structures would encourage their hydrolysis to UO_2F_2, and this would make their detection problematic without the availability of an appropriate environmental containment.

The particles in the samples of UO_2 and UO_2F_2 were discrete and well-shaped whereas the UO_3 particles were aggregates of submicron particles. A smaller particle size or higher surface area of the UO_3 samples might encourage better kinetics by increased probability of contact with NF_3, but the lowered onset temperature of the first exotherm should be related to the activation energy. The question arises as to what activates the NF_3 in the lower temperature regime. The reported bond dissociation energy for NF_3, $D(NF_2–F)$ of 238 kJ [41], is a bit greater than that of F_2 [42], and the enthalpy required to scission the first fluorine of NF_3 to produce an F radical between 200 and 1000 °C is approximately +250 kJ/mol. Extrapolation of reported equilibrium constant data [41] for the reversible reaction in

$$NF_3 \Longleftrightarrow NF_2^{\cdot} + F^{\cdot} \quad (3)$$

suggests that at equilibrium, the reaction at 700, 500, and 250 °C would produce approximately 3×10^{-4}, 8×10^{-6}, and 5×10^{-10} mol F per mol NF_3, respectively. If the extrapolation to 250 °C is creditable, the reaction would take over 1000 years at an NF_3 flow rate of 10 mL min^{-1} to react 20 mg of UO_3. Accordingly, it appears that a mechanism alternate to purely thermal dissociation of NF_3 is operative at the UO_3 surface and perhaps the submicron nature of the UO_3 particles or aspects of their crystallinity play a role in this reactivity.

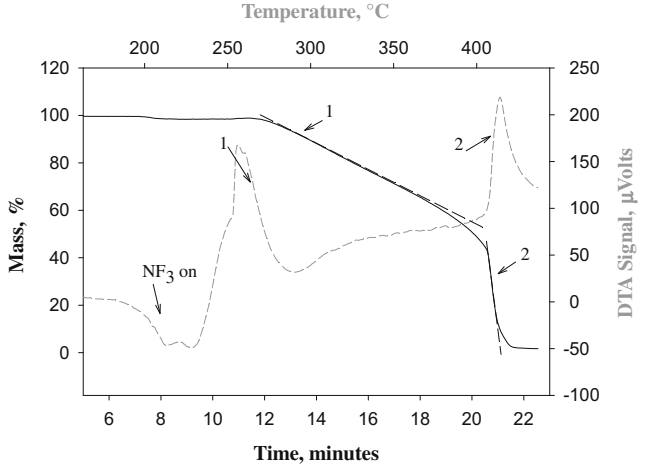

Fig. 3. The TG/DTA-measured thermal profile for the reaction of UO_3 powder and NF_3 at a sample heating rate of 2 °C min^{-1}. Two exothermic events marked (1) and (2) were observed; each produced UF_6. The experimental TG curve is plotted as the solid line, and the DTA curve is the dashed line.

3.4. NF_3 fluorination of α-U_3O_8 and β-U_3O_8

Fig. 4a shows the TG/DTA-measured thermal reactivity of α-U_3O_8 powder exposed to a flow of 5% NF_3 in argon gas. The sample heating rate was 10 °C min^{-1}. UF_6 was produced mostly from a single exothermic event with an onset temperature of 440 °C and a peak temperature of 520 °C. The thermodynamic data in Tables 1 and 2 for the enthalpy of formation of UF_6 from α-U_3O_8 predicts the observed exothermic behavior with an enthalpy just below that of UO_3. The plot of the DTA curve with respect to temperature (top axis) in Fig. 4a allows visualization of the rapid heat evolution as was commonly observed from these samples for sample heating

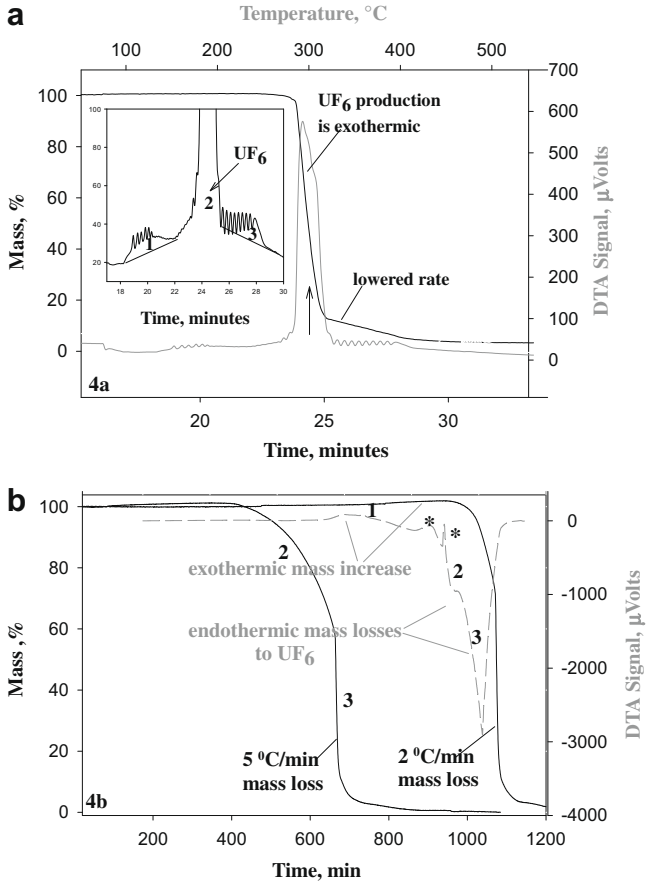

Fig. 4. (a) Thermal profile as measured by TG/DTA for the reaction of α-U_3O_8 powder and NF_3 at 10 °C min^{-1}. At the high-temperature side (3) of the reaction, a reduction in rate is indicated and implies the formation of a barrier to reaction or the presence of some rate limiting chemical intermediate. (b) Thermal profiles are plotted for 2 and 5 °C/min with respect to time on the *x* axis. The lower heating rate experiment was about 10 h in duration. The numbers 1, 2, and 3 relate rate changes in the mass curves to exothermic/endothermic events in the DTA signal. The experimental TG curves are plotted as solid lines, and the DTA curve is plotted as a dashed line.

rates above 10 °C/min. The inset in Fig. 4a shows an expanded view of the DTA curve to either side of the UF_6 production event. The oscillations of the sample pan reflect the coupling of two small thermal signatures, marked (1) and (3), to either side of the major thermal release of UF_6, marked (2). A uranium oxyfluoride had likely formed on the low-temperature side, and the decrease in the mass gradient toward the high-temperature side, marked (3) in Fig. 4a, is consistent with (exothermic) formation of a third product that was slightly rate limiting with respect to the UF_6 production.

In Fig. 4b is described a conspicuously more complex behavior that emerged with the use of lower sample heating rates. Fig. 4b is plotted with respect to time and shows mass gain and mass loss events at 2 and 5 °C/min. The 5 °C/min mass-loss curve required less time and as a result appears shorter in duration in Fig. 4b than the 2 °C/min experiment. The two mass-loss curves each suggest a low mass increase marked 1, followed by at least two different regimes of mass loss, marked 2 and 3. The later two resulted in visibly different rates of UF_6 production. The mass increase marked 1 was an exothermic one as recorded at 2 °C/min in the DTA curve. The two small exothermic peaks marked with asterisks were reproducible and so represent some physical or chemical change. The mass loss regimes marked 2 and 3 were unexpectedly and dominantly, endothermic.

There are a number of factors that could result in an endothermic or non-exothermic reaction. The possibilities include (1) a simultaneous endothermic event (sublimation of UF_6, melting point, or crystallinity change) which absorbs all heat produced, (2) the formation of UF_6 or an unknown volatile product, which escapes or is swept away before its heat of formation is transported to the detector, (3) the formation of an intermediate that decomposes endothermically to produce the volatile product UF_6, or (4) a combination of any of these possibilities. Currently, we have insufficient information to identify the incongruous phenomenon that is leading to the observation of exothermic events at higher heating rates and endothermic events at lower heating rates. Similar observations of endothermic reactions for fluorination of U_3O_8 with other fluorinating reagents have not been reported.

β-U_3O_8 is a high-temperature phase of α-U_3O_8 (orthorhombic). According to neutron diffraction data [43], the structure of β-U_3O_8 is pseudohexagonal or rigorously, orthorhombic. The reaction of NF_3 with β-U_3O_8 was similar to that of α-U_3O_8 with the exception that the onset temperature was about 100 °C higher using the same ramp rate of 10 °C min^{-1}. The experiment confirms that changes in crystallinity, particle size, surface area, and other physical characteristics can influence the reactivity of NF_3 with uranium materials. The SEM data do indicate that heating of the α-U_3O_8 to the β-U_3O_8 form caused an increase in the size of the particles from small to larger and elongated particles. These data are consistent with an interpretation wherein the crystal grains of α-U_3O_8 were sintered on heating and coalesced with other grains. As a result, larger particles of this more refractory β-U_3O_8 form were produced. Changes in particle size, one can rationalize, could change the rate of UF_6 production, but should not this greatly alter the onset temperature for conversion. Changes in crystallinity might change the onset temperature by allowing preferential attack along a crystallographic axis for instance, however, the crystallinity change between α-U_3O_8 and β-U_3O_8 is a rather subtle one [31,43].

3.5. NF_3 fluorination of UF_4

Fig. 5a provides the TG/DTA scans of a sample of UF_4 powder exposed to flowing 5% NF_3 in argon gas. The reaction was run at a sample heating rate of 10 °C min^{-1}, which resolved two exothermic events. The small exotherm near 400 °C and marked (1) in Fig. 5a signifies the initiation of UF_4 fluorination. At this heating

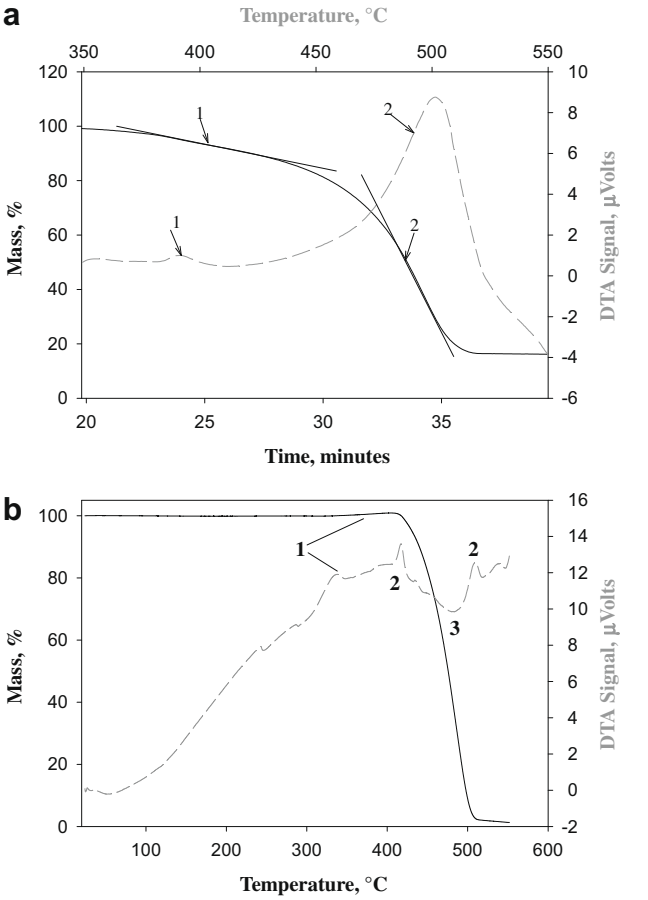

Fig. 5. (a) The TG/DTA-measured thermal profile for the reaction of UF_4 powder and NF_3 at a sample heat rate of 10 °C min^{-1}. Two exothermic events marked (1) and (2) were observed; each produced UF_6. The experimental mass-loss curve is plotted as the solid line, and the DTA curve is the dashed line. (b) At a sample heating rate of 2 °C min^{-1}, the exothermic events noted in (a) were discernable marked (1, 2) but the reaction to produce UF_6 became endothermic marked (3) as was described for the NF_3 reaction with α-U_3O_8.

rate, the event was coupled to a larger exothermic event near 500 °C that consumed 100% of the sample with concurrent release of UF_6. In the mass-loss curve, two distinct rates for UF_6 production are identified labeled as 1 and 2.

A mixture of green and black particles, present upon quenching the reaction along the region marked (1), indicated the formation of a stable intermediate, unidentified species involved in the conversion of UF_4 to UF_6. The observation is consistent with the formation of intermediate, uranium fluorides, U_2F_9 [44] and U_4F_{17} [13], as has been described by Labaton and Johnson [13] for F_2 fluorination of UF_4. A mass increase of about 1 wt% (along 1) was consistent with a low F/U ratio >4.25 or a compound with stoichiometry of U_4F_{17}. The XRD of the black product was notably different from the starting UF_4 but was not identifiable to our XRD databases.

Fig. 5b provides the TG/DTA scans at a sample heating rate of 5 °C min^{-1}. Slight mass gains associated with exothermic fluorination could be observed leading up to region 1. Near the area marked 2, exothermic mass loss began but the mass loss (3) associated with UF_6 production was overall endothermic. Finally, a small exotherm (also marked 2) appeared at higher temperature. The bimodal behavior for UF_6 production reproduces that discussed for fluorination of α-U_3O_8 and is exemplary for an endotherm superimposed on an exotherm. The two small exotherms marked as 2 are due to an exothermic source of UF_6 production

and the endothermic region marked 3, we speculate could represent sublimation of UF_6, heat loss from the purge, or alternately, a decomposition to UF_6 from a near-hexavalent fluorinated product, perhaps polymeric in nature. The very close resemblance of the U_3O_8 and UF_4 data at low sample heating rate suggest that the same fluorination event is produced and is in fact favored by the lowered heating rate.

A distinct black product was not observed in the XRD scans of quenched products formed from reaction between U_3O_8 and NF_3. It may be surmised from the data in Table 2 that compounds with F/U ratio <4.5 would react more exothermically than pentavalent or hexavalent uranium fluorides. The low F/U ratio, black product could be the origin of the small exothermic mass gain and exothermic mass loss in the UF_4 reaction. Because the formal oxidation state of U_3O_8 is a mixture of V and VI, compounds of F/U ratio <4.5 likely are not the source of the endothermic behavior seen for NF_3 fluorination of U_3O_8 and UF_4. These remarks then place the endothermic event observed for both U_3O_8 and UF_4 at higher oxidation state and higher fluoridation than compounds such as U_2F_9 [44] and U_4F_{17} [13]. Again we speculate sublimation of UF_6, heat loss from the purge, or decomposition to UF_6 from a near-hexavalent fluorinated polymeric product, are possibilities for further investigation. Similar data have not been reported for reaction of UF_4 with F_2. Although kinetic results were obtained from thermogravimetric mass-loss curves, enthalpy data were not discussed [19].

3.6. NF_3 fluorination of uranium metal

The reaction of uranium metal with NF_3 provides an example of metal catalyzed NF_3 reactivity. Fig. 6 shows the TG/DTA-measured thermal reaction profile of a sample of four uranium metal beads (9.0 mg) exposed to a flow of 5% NF_3 in argon gas. The reaction profile shown in Fig. 6 resulted from a heating ramp of 1 °C min^{-1}.

In this reaction, slight mass gains began as low as 60 °C. The reaction profile became strongly exothermic near 100 °C, peaking near 130 °C. Indeed, the sample size and heating rate had to be restricted below 10 mg and 2 °C/min, respectively, because of the rapid kinetics and excessive heat of the reaction; in larger mass experiments (>10 mg) NF_3 appeared to directly convert the uranium metal to UF_6 as the reaction heat raised the sample's temperature to near 500 °C. At 148 °C, the mass of the sample had increased to about 4.7 wt% below theoretical for UF_4 formation. A second sample was rerun to 150 °C and cooled. An XRD powder pattern was taken of the thermochemically-pulverized material. The XRD scan was consistent with complete conversion of the metal sample to UF_4. SEM micrographs indicated that the particles of UF_4 ranged from 0.1 to 2 μm.

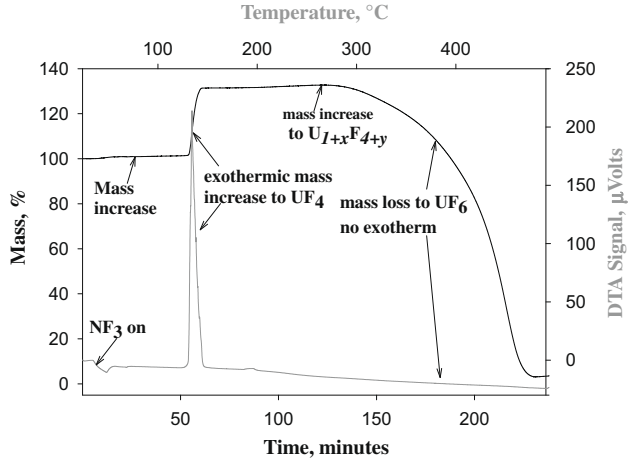

Fig. 6. The TG/DTA-measured thermal profile for the reaction of uranium metal and NF_3 at a sample heating ramp of 1 °C min^{-1}. The reaction began producing UF_4 below 100 °C. Above 200 °C, fluorination continued. Below 2 °C min^{-1}, the exotherm for UF_6 production near 300 °C was not observed even though the mass loss, indicating production of UF_6, was quite abrupt. The experimental mass-loss curve is plotted as the solid line, and the DTA curve is the dashed line.

Above 288 °C, the mass continued to increase to greater than the theoretical mass limit of UF_4 to where production of UF_6 began. The production of UF_6 from the thermal UF_4 product from reaction of NF_3 with U metal, was similar to that of the reaction of $UF_4.2H_2O$ from house stocks discussed above. For U metal, the reaction observed by the TG was observed to be neither exothermic nor endothermic in contrast to the calculated exothermicity (Table 2) and observed for stock UF_4.

The major stepwise reactions for UF_6 production from the metal are shown in Eqs. (4). The production of nitrogen is assumed here for metrical purposes. The overall enthalpy of formation of UF_6 is listed in Table 1 (Eq. 6) and is at least twice greater than those calculated for the U(IV, VI) oxides. The calculated reaction heats for the stepwise reactions predict that most of the exothermic behavior should be due to the oxidation of U metal to UF_4. This expectation was borne out during TG/DTA experiments with formation of UF_6 from UF_4, for which there was no heat production observed at 2 °C min^{-1}, relative to the intense local heating observed in the formation of UF_4 from uranium metal.

$$\begin{aligned} U + \frac{4}{3}NF_{3(g)} &= UF_4 + \frac{2}{3}N_{2(g)} \\ UF_4 + \frac{2}{3}NF_{3(g)} &= UF_6(g) + \frac{1}{3}N_{2(g)} \end{aligned} \tag{4}$$

We have noted that the reaction of NF_3 with uranium metal tends to be strongly exothermic. The data in Table 1 predict the observation. The thermodynamic prediction does not account for the observed low onset temperature of the reaction. As discussed above, the extent of the thermal dissociation of NF_3 at 60 °C would be so small as to take 10^9 yr to react 9 mg of uranium metal [41]. The reactivity is therefore more consistent with a surface facilitated mechanism such as dissociative chemisorption or dissociative electron capture of NF_3 [45–50] or its dimer N_2F_4 on the uranium metal surface.

4. Conclusions

Our thermoanalytical studies have shown that NF_3 reacts with a variety of uranium compounds to produce the industrially important UF_6. While these studies are not complete, they indicate that NF_3 offers promise as a replacement fluorinating agent for uranium and other nuclear materials that form volatile fluorides such as neptunium and plutonium. NF_3 in this way could find application in the production of UF_6 from recovered uranium during conventional reprocessing. Reactions with NF_3 offer generally safer access to fluorination studies with the potential to improve fundamental understanding of the reactivity between actinides and fluorinating agents and a deeper understanding of actinide/fluorine interactions.

We have presented TG/DTA reaction profiles for the reaction of NF_3 with uranium metal, UO_2, UF_4, UO_3, U_3O_8, and $UO_2F_2{\cdot}2H_2O$. Calculated enthalpies and free energies of formation of UF_6 from these compounds predict a correlation with the uranium oxidation state and this was qualitatively observed in the TGA experimental data. The reactions of NF_3 with the uranium oxides were consistent with stepwise formation of UO_2F_2 and higher fluoridation intermediates. Similar onset temperatures and reactivity have been described for the reaction of fluorine with uranium oxides [31,33–39]. Our studies of uranium metal and UF_4 with NF_3 implicate the formation of higher fluoridation intermediates such as UF_5,

U_2F_9, and U_4F_{17} in a fashion similar to the hyperstoichiometric oxidising of uranium, such as found in U_3O_7 and U_4O_9. Several of the observed thermal behaviors for reaction of NF_3 with the uranium compounds described here have not been reported for the F_2 reaction with the same uranium compounds. It is not yet understood if the disparity is caused by the fluorination reagent or differences in experimental conditions.

A reoccurring theme in the reactions of NF_3 with uranium metal, UO_2, and UO_3 are lowered onset reaction temperatures at which initial reaction behaviors were observed. For the cases of UO_2 and UO_3, formation of UF_6 could be observed below 250 °C. For uranium metal, the addition of NF_3 was exothermic below 130 °C. The reactivity described for the reaction of NF_3 and uranium metal hints at a NF_3 decomposition mechanism inspired by surface-assisted activation of NF_3 through intermediates such as the tetrafluoro dimer, N_2F_4. In the absence of moisture the surface sorbed dimer might lose fluorine sequentially to produce dinitrogen.

Heat release during UF_6 production often will exceed 100 °C min^{-1} per 20 mg of sample at fast sample heating rates. The local heating accelerates UF_6 production and in turn potentially dissociates intermediates, which might otherwise form at times of less than a few minutes under our experimental conditions. Low sample heating rates and isothermal heating are thermal probes for investigation of fluorination reaction sequences with lower heat production. Chemical modeling and product analysis by coupled TG-MS techniques are currently being pursued for uranium, as well as other materials relevant to fuel processes.

Acknowledgments

The authors gratefully acknowledge the support of the US Department of Energy for the support to evaluate alternate technologies for the characterization and removal of solid uranium and technetium deposits at the Portsmouth Gaseous Diffusion Plant. Pacific Northwest National Laboratory is operated for the US Department of Energy by Battelle under Contract DE-AC05-76RL01830.

References

[1] J.J. Schmets, At. Energy Rev. 8 (1970) 3–126.
[2] V.V. Shatalov, M.B. Seregin, At. Energ. 90 (3) (2001) 224–234.
[3] M. Koamoshida, F. Kawamura, T. Sawa, J. Yamashita, Prog. Nucl. Energ. 37 (2000) 145–150.
[4] A.A. Chilenskas, Nucl. Appl. 5 (1968) 11–19.
[5] A.A. Jonke, At. Energy Rev. 3 (1965) 3–60.
[6] N.M. Levitz, USAEC-Report ANL-7583, 1969.
[7] N.P. Galkin, L.A. Ponomarev, Yu. D. Shishkov, Radiokhim. 22 (5) (1990) 754–757.
[8] M.J. Stephenson, J.R. Merriman, H.L. Kaufman, USAEC-Report K-1713, 1966.
[9] G.D. Del Cul, A.S. Icenhour, D.W. Simmons, L.D. Trowbridge, in: Presentation at the American Nuclear Society Fifth Topical Meeting on Spent Nuclear Fuel and Fissile Materials Management, 2002, pp. 17–20.
[10] R.D. Scheele, B.K. McNamara, B.M. Rapko, M.K. Edwards, A.E. Kozelisky, R.C. Daniel, T.I. McSweeney, S.J. Maheras, P.J. Weaver, K.J. Iwamasa, R.F. Kefgen, Development of NF_3 deposit removal technology for the Portsmouth gaseous diffusion plant, in: Proceedings of Waste Management 06, Tucson, AZ, 2006.
[11] M. Iwasaki, J. Nucl. Mater. 22 (2) (1968) 216–226.
[12] M. Iwasaki, J. Inorg. Nucl. Chem. 26 (1964) 1853–1861.
[13] V.Y. Labaton, K.D.B. Johnson, J. Inorg. Nucl. Chem. 10 (1959) 74–85.
[14] T. Yahata, M. Iwasaki, J. Inorg. Nucl. Chem. 26 (1964) 1863–1867.
[15] V.Y. Labaton, J. Inorg. Nucl. Chem. 10 (1958) 86–93.
[16] T. Sakurai, J. Phys. Chem. 78 (1974) 12.
[17] K.C. Kim, G.M. Campbell, Appl. Spectrosc. 39 (1985) 625–628.
[18] J.G. Maim, P.G. Eller, L.B. Asprey, J. Am. Chem. Soc. 106 (1984) 2726–2727.
[19] A.G. Streng, Chem. Rev. 63 (1963) 607–624.
[20] A.B. Burg, Volatile inorganic fluorides, in: J.H. Simmons (Ed.), Fluorine Chemistry, vol. 1, Academic Press, Inc., New York, NY, 1950.
[21] F. Ishii, Y. Kita, in: T. Nakajima, B. Zemva, A. Tressaud (Eds.), Advanced Inorganic Fluorides, Elsevier, Amsterdam, 2000, p. 629.
[22] J.A. Barkanic, B. Golja, Microelectron. J. 16 (1) (1985) 5–20.
[23] B. Golja, J.A. Barkanic, Hoff, J. Stach, The Electrochemical Society Extended Abstracts, Washington, DC, October 9–14, 1983, pp. 207–208.
[24] J.G. Langan, S.W. Rynders, B.S. Felker, S.E. Beck, J. Vac. Sci. Technol. A 16 (1998) 2108–2114.
[25] B.E.E. Kastenmeier, G.S. Oehrlein, John G. Langan, William R. Entley, J. Vac. Sci. Technol. A 18 (2000) 2102–2107.
[26] R.E. Anderson, E.M. Vander Wall, R.K. Schaplowsky, USAF Propellant Handbooks, vol. 3, Part A. Nitrogen Trifluoride, Systems Design Criteria, ADB028448, AeroJet Liquid Rocket Co, Sacramento, California, 1978.
[27] M. El-Genk, Nucl. Technol. 132 (2) (2000) 290–308.
[28] J.M. Veilleux, M.S. El-Genk, E.P. Chamberlin, C. Munson, J. FitzPatrick, J. Nucl. Mater. 277 (2000) 315–324.
[29] P.W. Wilson, Pure Appl. Chem. 22 (1972) 1–12.
[30] ICDD data base-PDF-4, International Centre for Diffraction Data, Newtown Square, PA 19073-3273, USA, 2007.
[31] B.O. Loopstra, Acta Cryst. B26 (1970) 656–657.
[32] A. Roine, Outokumpto HSC Chemistry Chemical Reaction and Equilibrium Software (HSC-5), Outokumpto Research Oy, ISBN 952-9507-08-9, 2002.
[33] S. Ogata, S. Homma, A. Sasahira, F. Kawamura, J. Koga, S. Matsumoto, J. Nucl. Sci. Technol. 41 (2) (2004) 135–141.
[34] R.T. Paine, R.R. Ryan, L.E. Aspery, Inorg. Chem. 14 (1975) 1113–1117.
[35] P.A.G. O'Hare, J.G. Malm, J. Chem. Thermodyn. 14 (1982) 331–336.
[36] K.H. Lau, R.D. Brittain, D.L. Hildenbrand, J. Phys. Chem. 89 (1985) 4369–4373.
[37] P.A. Wilson, J. Chem. Soc. Chem. Comm. 22 (1972) 1241–1243.
[38] D.P. Armstrong, R.J. Jarabek, W.H. Fletcher, Appl. Spectrosc. 43 (1989) 461–468.
[39] P.A. Wilson, J. Inorg. Nucl. Chem. 36 (1974) 1783–1785.
[40] M.G. Ortey, R.A. Le Doux, J. Inorg. Nucl. Chem. 29 (1967) 2249–2256.
[41] P.J. Evans, E. Tschuikow-Roux, Chem. Phys. 65 (1976) 4202–4209.
[42] G.D. Zhou, K.T. Chou, W. Chen, Fundamentals of Structural Chemistry, World Scientific Publishing Company, 1993. The bond dissociation energy of F_2, D(F–F) = 155 kJ/mol.
[43] R. Herak, Acta Cryst. B25 (1969) 2505.
[44] W.H. Zachariasen, Acta Cryst. 2 (1949) 390.
[45] G.L. Schott, L.S. Blair, J.D. Morgan Jr., J. Phys. Chem. 77 (1973) 2823–2830.
[46] K.O. MacFadden, E. Tschuikow-Roux, J. Phys. Chem. 77 (1973) 1475–1478.
[47] C.B. Colburn, A. Kennedy, J. Chem. Phys. 35 (1961) 1892.
[48] F.A. Johnson, C.B. Colburn, J. Am. Chem. Soc. 83 (1961) 3043.
[49] R.M. Reese, V.H. Dibeler, J. Chem. Phys. 24 (1956) 1175.
[50] J.C.J. Thynne, J. Phys. Chem. 75 (1969) 1586–1588.